Int. j. adv. multidisc. res. stud. 2026; 6(6):864-872

Received: 30-09-2026
Accepted: 10-11-2026

International Journal of Advanced Multidisciplinary Research and Studies

ISSN: 2583-049X

When Different Mechanisms Produce Similar Diffraction Signals: Model Identifiability in Near-Bragg Scattering

Konstantinos T Kotsis
Lab of Physics Education and Teaching, Department of Primary Education, University of Ioannina, Greece

Corresponding Author: **Konstantinos T Kotsis**

Abstract
Weak scattering features near a Bragg reflection can be compatible with multiple physical mechanisms when angular acceptance, energy integration, and instrumental response suppress their distinguishing characteristics. This critical methodological synthesis re-examines documented diffraction observations from a 1986 doctoral investigation and connects them with structural and practical identifiability theory. The archival evidence challenges a particular simple thermal-scattering benchmark and demonstrates preparation sensitivity, but it does not independently resolve elastic and inelastic intensity fractions or identify a unique defect population. Exact two-component analysis shows that coincident measured response functions identify only an amplitude sum; an equal-width Gaussian illustration quantifies the deterioration of conditioning as component overlap increases. A temperature-contrast example demonstrates recovery of two amplitudes under constrained normalization and background, while also exposing the non-identifiability introduced by an unknown constant background. We extend these results to the role of nuisance-parameter sensitivity and formulate a diffraction-specific strategy for selecting energy, reciprocal-space, temperature, surface-treatment, and instrumental-reference measurements. These analyses are theoretical illustrations, not refits of historical scans or new experimental observations. The central contribution is an explicit correspondence between experimentally accessible contrasts, the degeneracies they may resolve, and the assumptions needed for defensible mechanism attribution.

Keywords: X-ray Diffraction, Near-Bragg Scattering, Thermal Diffuse Scattering, Surface Defects, Instrumental Resolution

1. Introduction

An additional maximum in a high-resolution diffraction scan is an observation; its assignment to a microscopic process is an inference. The distinction becomes consequential near a reciprocal-lattice point, where dynamical diffraction, static displacement fields, thermal motion, surface termination, and the instrument response may contribute to closely overlapping signals. A recognizable peak position or an apparently characteristic intensity dependence can narrow the set of explanations without selecting a unique one. The central problem is therefore whether the available measurements contain the independent information required to distinguish the proposed mechanisms.

This problem arises naturally from the doctoral investigation of dynamical and kinematical X-ray scattering near a reciprocal-lattice point reported by Kotsis [1]. The thesis examined additional diffraction features using multi-crystal arrangements and considered their angular behavior, intensity dependence, and sensitivity to specimen preparation. Related publications addressed the use of kinematical diffraction in topography, diffraction near the Bragg angle for an asymmetrically cut crystal, and spurious peaks produced within a multi-crystal spectrometer [2-4]. Together, these studies provide a historically situated example of the difficulty of assigning weak features when several physical processes interact with the measurement geometry.

The present contribution revisits that difficulty as an inverse problem. It does not seek another fitted power law from the historical tables or a new estimate of a thermal fraction. Instead, it asks what kind of inference the preserved observations support, why some decompositions remain ambiguous, and which additional measurements could make alternative explanations distinguishable. This focus allows an older experimental investigation to support a new methodological synthesis without presenting its observations as newly acquired data.

The distinction matters because later theory and experiments show that thermal diffuse scattering close to a Bragg condition cannot always be represented by a smooth kinematical background. Juretschke [5] predicted structured thermal-scattering

distributions within a Bragg region, and Mitsui *et al*. [6] reported incident-angle-dependent thermal-scattering behavior in Si 111. These findings do not retrospectively identify the origin of a particular historical peak. They do show why rejection of an elementary thermal model must be stated at the level of that model rather than extended automatically to every thermal contribution.

Three connected questions guide this synthesis. What is identifiable when two mechanisms generate the same measured angular response? How does finite resolution affect separability when the intrinsic responses differ? What experimental contrasts add independent information after nuisance parameters are taken into account? Answering these questions places the historical evidence within a framework that distinguishes observational reliability, model adequacy, parameter estimation, and physical attribution.

The contribution of this study is therefore not a new claim about the microscopic identity of the historical peak. Rather, it is a diffraction-specific account of three inferential steps that are often conflated: Demonstrating that a proposed forward model fails, establishing that parameters within an alternative model can be estimated, and discriminating among physically different models after their predictions have passed through the same measurement operator. A distinctive practical outcome is a conditional measurement-design matrix linking each proposed experimental contrast to both the information it adds and the nuisance effects capable of cancelling that information. The analytical constructions make this logic explicit while deliberately avoiding an unsupported quantitative reconstruction of the archival instrument.

2. Theoretical Background

Near-Bragg scattering must be interpreted with attention to the wavefields that develop inside a nearly perfect crystal. Dynamical diffraction describes interactions that are absent from a simple independent-scattering picture, including extinction and the coupling of incident and diffracted fields [7]. Current numerical implementations of perfect-crystal Takagi–Taupin equations make these effects accessible for forward calculations, although their availability does not remove the need to specify specimen geometry and boundary conditions correctly [8]. A more sophisticated calculation can improve the physical model while leaving its parameters poorly constrained by a particular experiment.

Thermal and static diffuse scattering also share aspects of their long-wavelength behavior. In an appropriate acoustic, classical limit, a thermal diffuse intensity can have an inverse-square dependence on the distance from a reciprocal-lattice point. Static elastic displacement fields around defects can exhibit a similar leading dependence in a Huang-scattering regime [9]. Such similarity is conditional on direction, polarization, the displacement field, and the range of validity of the approximation. It is consequently inappropriate to treat an inverse-square trend, by itself, as a unique signature of thermal motion or static disorder.

For reciprocal-space displacement $q = Q - G$ from a reciprocal-lattice vector G, a schematic near-Bragg comparison may be written as:

$$q = Q - G$$

$$I_s(q, \varphi) \propto H(\varphi) / |q|^2 \text{ and } I_t(q, \varphi, T) \propto T\, P(\varphi) / |q|^2$$

The first expression represents a static strain-related Huang-like contribution, whereas the second represents a classical acoustic thermal contribution. Here H and P denote distinct, model-dependent directional factors, and φ is an azimuthal coordinate. These proportionalities apply only within restricted asymptotic regimes; they are not universal scattering laws and omit dynamical diffraction, finite-size effects, and the full phonon spectrum. Their purpose is to show why measuring only one radial line may not distinguish amplitudes even when different azimuths or reflections could reveal distinct directional structure. A credible physical simulation would require material-specific elastic constants, phonon eigenvectors, defect displacement fields, boundary conditions, and a calibrated resolution operator; these quantities are unavailable for a reconstruction of the archival measurements.

Surface-related scattering introduces additional possibilities. Crystal truncation produces intensity extended along reciprocal-space directions related to the surface normal, and surface roughness modifies that distribution [10]. Surface relief can also require a dynamical treatment in high-resolution triple-crystal measurements [11]. These results establish that surface structure can affect diffraction in several physically different ways. They do not justify equating every preparation-sensitive feature with a particular defect population or with a universal surface-scattering exponent.

Thermal scattering itself is modified by diffraction conditions. The calculations of Wasserstein-Robbins and Juretschke [12] show that the interaction of phonon scattering and dynamical wavefields can generate angular structure. The explicit Ge 220 example in the latter study should not be transferred quantitatively to a Ge 111 experiment without a new forward calculation. More recently, Schmidt *et al*. [13] demonstrated an interplay between compositional disorder and lattice dynamics in mixed alkali halides. That different material system provides a reason to examine coupling between static disorder and thermal response, rather than assume that an intervention changes only one component.

The instrument adds another layer between mechanism and observation. A triple-crystal arrangement selects a region of reciprocal space through the coupled responses of its crystals, source, and detector. Lucas *et al*. [14] investigated the resolution function experimentally and theoretically, including departures from a Gaussian description in the wings. A narrow observed maximum can therefore reflect a combination of specimen scattering and instrumental selection. The historical demonstration of spurious peaks in a multi-crystal spectrometer is particularly relevant: Structured features can arise through angular separation within the optical arrangement, so an instrumental alternative need not be a featureless background [4].

For a restricted two-component intensity model, a useful schematic forward relation is:

$$y_e = \mathcal{R}_e[D_e(\eta) + a_s f_{s,e} + a_t f_{t,e}] + b_e + \varepsilon_e \qquad (1)$$

Here, y denotes the observations in experimental condition e; D is a modeled diffraction contribution; f_s and f_t describe proposed static and thermal contributions with amplitudes a_s and a_t; η denotes additional physical or instrumental parameters; $\mathcal{R}$ is the measurement operator; b is background; and ε represents measurement error. The

operator can include angular and energy acceptance, geometry, and averaging. It need not be a shift-invariant convolution. Additivity of component intensities is an assumption appropriate to specified incoherent or ensemble-averaged contributions. Where coherent amplitudes interfere, the amplitudes and their cross terms must instead be modeled explicitly.

For clarity, the schematic observation model should be understood as $y_e = \mathcal{R}_e[D_e(\eta) + a_s f_{s,e} + a_t f_{t,e}] + b_e + \varepsilon_e$, where $\mathscr{R}_e$ is a condition-dependent linear measurement operator only when the chosen intensity-addition approximation is justified. The forward map must be expanded at the complex-amplitude level if coherent interference or coupling invalidates simple intensity additivity. In either case, parameters are identified from the predicted recorded counts, not from unbroadened theoretical functions considered independently of the instrument.

Identifiability concerns whether different admissible parameter values can generate the same observations under the chosen forward model. Structural non-identifiability persists even with ideal, error-free observations of the specified kind. Practical non-identifiability arises when the available observations constrain parameters too weakly at the actual noise level and sampling range [15, 16]. These distinctions are conditional on the model and the observation scheme. A parameter can be identifiable within an inadequate model, while two physically different models can make indistinguishable predictions over the measured domain.

Local sensitivity provides one way to examine the problem. For a linear amplitude model, the columns of the design matrix are the observed component responses. Identical columns imply an exact ambiguity. Nearly parallel columns imply that small errors can produce large changes in the estimated decomposition. In nonlinear models, a local full-rank Jacobian is not, by itself, a proof of global uniqueness; regularity assumptions and alternative parameter regions must also be considered [17]. Profile likelihood can expose weakly constrained directions that an uncertainty calculation based only on local curvature may conceal [15, 16].

A useful refinement is to partition the local sensitivity matrix into target parameters $a = (a_s, a_t)$ and nuisance parameters η, writing:

$$J = [J_a \; J\eta]$$

Under a positive-definite statistical weighting matrix W, the information relevant to a after allowing nuisance adjustment is the Schur-complement expression:

$$F_{a|\eta} = J_a^T W J_a - J_a^T W J\eta \, (J\eta^T W J\eta)^{-1} J\eta^T W J_a$$

This expression requires the nuisance information matrix to be invertible. Equivalently, it measures target sensitivity remaining after projection away from directions explainable by nuisance changes. A nearly singular $F_{a|\eta}$ signals weak conditional separation, even if J_a alone has independent columns. If the inverse does not exist, generalized-inverse or explicit reparameterization methods are needed; rank and global uniqueness must still be examined separately. This formulation makes background, normalization, angular-zero drift, and resolution-width uncertainty part of the identifiability analysis rather than afterthoughts.

3. Method

The study adopts a critical secondary-synthesis design. Its empirical anchor is the thesis of Kotsis [1], with emphasis on the thermal-scattering comparison on printed pages 181–183 and the surface-treatment observations on printed pages 190–193. The associated articles by Alexandropoulos and Kotsis [2] and Kotsis and Alexandropoulos [3, 4] supply context for diffraction geometry, applications, and instrumental alternatives. The thesis and related publications belong to a connected research program and are not treated as independent replications. The synthesis combines archival interpretation with analytical examples derived for the present article.

The literature was chosen purposively according to its specific inferential role: Foundational dynamical-diffraction and diffuse-scattering sources establish the competing physical mechanisms; publications related to the historical apparatus describe specimen and instrumental alternatives; later work documents structured thermal and surface-related responses; and identifiability studies provide mathematical criteria for interpreting competing forward models. The selected sources were assessed for whether they establish a predicted observable, characterize an instrumental transformation, or clarify the uniqueness and stability of inference. This is a critical methodological synthesis, not a systematic search, meta-analysis, independent replication, or comprehensive inventory of every near-Bragg mechanism. Selection does not imply that all relevant physical alternatives have been exhausted.

Historical observations were interpreted at the level of the measured observable and its documented experimental contrast. Peak direction was distinguished from peak height, preparation sensitivity from microscopic defect identification, and angular discrimination from energy discrimination. The thesis comparison with a simple thermal-scattering prediction was assessed as a test of that particular prediction. Surface treatment was considered an intervention with potentially multiple consequences, including changes in strain, surface structure, alignment, and wavefield propagation. No new uncertainties, independent scan replicates, or elastic-to-inelastic fractions were assigned to the archive.

The archival evidence was extracted as reported contrasts rather than as reconstructed measurements. The available material distinguishes the Si 220 rubbing observation, the Ge 111 sequence of CP-4 polishing treatments, and the comparison with a restricted thermal angular prediction. The present manuscript does not supply original count series, uncertainty estimates, illuminated-volume calibrations, or full angular resolution functions. In the absence of those records, it would be inappropriate to report treatment-effect magnitudes, fit newly chosen scattering exponents, or infer absolute elastic and inelastic fractions. The resulting evidence table consequently distinguishes what was directly observed, what model-specific conclusion follows, and what remains untested.

The analytical component first considers two response functions that become identical after measurement. It then examines two unit-normalized Gaussian response functions separated by Δ and sharing an effective standard deviation σ. Their overlap and the condition number of the two-column design operator are calculated exactly using continuous, unweighted inner products. This construction

illustrates the effect of overlap under a specified metric. It is not a fitted resolution model for the historical diffractometer, and it does not assume that actual near-Bragg profiles are Gaussian.

The final analytical example uses a deliberately restricted temperature-response model. A temperature-independent contribution S and a classical thermal term CT are assumed to share an angular response. Two measurements at distinct known temperatures are considered under stable normalization and independently known background. The example is then expanded to include an unknown constant background, showing which ambiguity remains. The proposed experimental contrasts are assessed by whether their predictions add independent parameter sensitivity after plausible nuisance effects are included. All numerical values and plotted curves in the analytical illustrations are constructed examples, not additional thesis measurements.

For prospective measurement design, the two-component forward map can be evaluated over several experimental conditions e by stacking recorded-response vectors. This increases information only if at least one new condition changes a relative response in a way not reproducible by admissible adjustments of shared or condition-specific nuisance parameters. Where counts are recorded, a Poisson likelihood with a calibrated or separately estimated background would usually be preferable to the continuous unweighted metric used in the illustrative Gaussian derivation. No historical detector-counting distribution is reconstructed here. All analytical values in Table 2 and Figures 1–2 are reproducible directly from the stated formulae:

$$\rho(d) = exp(-\frac{d^2}{4})$$

$$\kappa(d) = \sqrt{\frac{1 + \rho(d)}{1 - \rho(d)}},\ d > 0$$

At the limiting case $d = 0$, the two-column design operator has rank one.

4. Results

The archival evidence constrains the interpretation in several ways without providing a complete component decomposition. The thesis reports an additional feature whose angular behavior did not follow the trajectory predicted by the simple thermal-scattering comparison considered there. It also reports that rubbing the Si 220 specimen increased the additional feature and that successive CP-4 polishing treatments reduced the corresponding feature in Ge 111 [1, pp. 181–183, 190–193]. These are different specimen and reflection conditions. Their directions of change should not be pooled into a common treatment effect or interpreted as a shared quantitative response coefficient.

For transparency, the archival evidence should be read at the level documented by the historical sources: Si 220 rubbing and Ge 111 CP-4 polishing were not matched interventions on a common specimen or reflection. The different preparation histories, materials, and scattering geometries preclude a pooled effect estimate. Likewise, the mismatch with the historical thermal benchmark pertains to that benchmark's particular angular prediction and cannot exclude modern dynamical thermal-scattering calculations. A direct archival curve, if subsequently recovered and its provenance verified, would provide useful visual corroboration, but no such curve is fabricated or digitally reconstructed in this paper.

Table 1: Inferential scope of the historical observations

Historical observation	Supported inference	Remaining ambiguity
Additional-peak direction differs from the simple thermal benchmark	Challenges that specified angular prediction	Does not exclude dynamical thermal scattering in general
Rubbing increases the additional feature in Si 220	Feature is sensitive to the preparation intervention	Defect scattering, strain, relief, and optical coupling are not separated
CP-4 polishing reduces the feature in Ge 111	Feature responds to successive surface preparation	No independently measured defect density or elastic fraction
Multi-crystal optics can generate secondary features	A structured instrumental alternative must be considered	Peak shape alone does not establish a specimen origin

Note: The first three rows synthesize Kotsis [1, pp. 181–183, 190–193]. The last row draws on Kotsis and Alexandropoulos [4]. The two preparation experiments concern different specimens and reflections; they are not pooled.

The observations therefore support a preparation-sensitive contribution and challenge a restricted thermal account. They do not establish that the full signal is elastic, that every thermal model fails, or that a single surface-defect species is responsible. The absence of energy-resolved component measurements is decisive for the scope of the inference. The historical interpretation remains physically informative, but its strongest defensible formulation concerns the observations and the models tested, rather than a uniquely measured partition of mechanisms.

An exact ambiguity follows immediately when the observed component functions coincide. If the static and thermal responses both equal f at all sampled coordinates, the background-corrected model becomes:

$$y = (a_s + a_t)f = Af \quad (2)$$

Only A, the sum of the amplitudes, is identified. Every pair a_s + c and a_t − c produces the same observations whenever both amplitudes remain admissible. If nonnegativity is imposed and A is known, the possible static amplitude remains anywhere between zero and A. Positivity limits the family of solutions but does not select one. Additional points along the same common response, longer counting times, or repeated scans under the same condition do not change this exact rank-one structure.

The distinction between exact ambiguity and weak separation becomes visible when the response functions differ slightly. Let f and g each have unit squared integral and let their overlap be ρ. The Gram matrix of the two-column design operator J is:

$$J^T J = \begin{bmatrix} 1 & \rho \\ \rho & 1 \end{bmatrix} \quad (3)$$

For $0 \le \rho < 1$, its eigenvalues are $1 + \rho$ and $1 - \rho$. The ratio of the largest to the smallest singular value of J is therefore:

$$\kappa(J) = \sqrt{\frac{1 + \rho}{1 - \rho}} \quad (4)$$

The condition number diverges as the functions become identical. In this linear, unweighted example, it measures sensitivity of the amplitude decomposition to perturbations under the stated normalization. It is not a universal identifiability score and does not replace a likelihood analysis with the actual counting statistics, background uncertainty, and instrument calibration.

This expression also requires care in its physical interpretation. The condition number pertains to a two-column linear operator with equal unit-norm columns and the specified inner product. Its magnitude is not an experimental signal-to-noise ratio, and there is no universal condition-number boundary separating 'identifiable' from 'unidentifiable' diffraction mechanisms. Under finite angular sampling, Poisson heteroscedasticity, unknown background, and calibration uncertainty, the weighted likelihood geometry may differ substantially. Thus Table 2 quantifies sensitivity to overlap under an idealized observation scheme, not a minimum angular separation required by a particular instrument.

For Gaussian functions of equal effective width, the normalized overlap is:

$$\rho = exp(-\frac{\Delta^2}{4\sigma^2}) \quad (5)$$

Writing d = Δ/σ makes the illustration dimensionless. Table 2 reports the resulting overlap and condition number. A separation of one effective standard deviation gives a condition number of approximately 2.84, whereas a separation of one tenth of that width gives approximately 28.3. At zero separation, the two-amplitude model has rank one. For any positive separation, it has rank two under this ideal continuous observation scheme, although practical estimation may remain unreliable.

Table 2: Conditioning of two ideal Gaussian component responses

Separation / width, d	Overlap, ρ	Condition number, κ(J)	Rank
0.00	1.000000	Unbounded	1
0.10	0.997503	28.28	2
0.25	0.984496	11.31	2
0.50	0.939413	5.66	2
1.00	0.778801	2.84	2
2.00	0.367879	1.47	2

Note: Calculated for two unit-norm Gaussians with equal effective width, continuous observation over the full coordinate axis, and unweighted inner products. These are illustrative mathematical values. Practical estimation also depends on counting statistics, scale, sampling, and nuisance parameters.

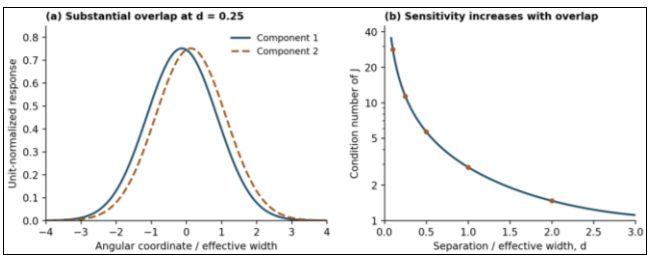


Fig 1: Overlap and conditioning in a constructed two-component model

Note: Analytical illustration, not experimental data. Panel (a) shows two unit-L²-norm Gaussians separated by 0.25 effective standard deviations. Panel (b) gives the singular-value condition number of their two-column design operator. Markers correspond to nonzero separations in Table 2. No universal adequacy threshold is implied.

If an intrinsic Gaussian profile is convolved with a Gaussian instrument response, the squared effective width is the sum of their squared widths. Increasing the response width at fixed intrinsic separation reduces d and increases the overlap. Fig 1 illustrates the resulting loss of distinguishing shape information. Real multi-crystal resolution can have non-Gaussian wings and angular–spectral correlations; consequently, the example establishes a mathematical possibility and a direction of sensitivity, rather than an empirical resolution threshold for the archive.

An experimental resolution function cannot generally be replaced by a single Gaussian without validation. In a triple-crystal experiment, acceptance may be asymmetric, have substantial tails, and couple angular and spectral coordinates. Consequently, an informative practical extension would propagate two physically specified specimen-scattering predictions through the same measured multi-dimensional response before comparing their identifiability. A Gaussian convolution remains useful here only because it isolates one exact mechanism for loss of shape information under controlled mathematical assumptions.

Temperature contrast can remove the common-shape amplitude ambiguity in a restricted model even when angular separation is unavailable. Suppose a registered, background-corrected response amplitude satisfies:

$$Y(T) = S + CT \quad (6)$$

At two temperatures, the design matrix has rows $(1, T_1)$ and $(1, T_2)$. Its determinant is $T_2 - T_1$, so distinct temperatures provide two independent equations for S and C. The solution is:

$$C = \frac{Y_2 - Y_1}{T_2 - T_1}, \quad S = \frac{T_2 Y_1 - T_1 Y_2}{T_2 - T_1} \quad (7)$$

This is an analytical identifiability result, not a claim that two temperatures are sufficient for a reliable physical experiment. The assumed linear thermal response must hold over the selected range, the response shape must remain appropriately modeled, and temperature-induced changes in the specimen and instrument must be controlled. Repeated measurements at additional temperatures are valuable for assessing those assumptions and estimating uncertainty.

The assumed C T term is most defensible as a local classical-limit approximation to an acoustic phonon contribution, not as a general law for measured near-Bragg peak height. A heating series can also modify lattice spacing, Debye–Waller attenuation, absorption, static disorder, and internal dynamical wavefields. Accordingly, a meaningful temperature study would track a reference reflection, monitor incident flux, measure heating and cooling trajectories, and fit temperature-specific offsets or response changes only when those nuisance degrees of freedom are supported by independent controls. The determinant argument proves algebraic uniqueness for a

deliberately restricted model; it does not prove physical specificity in an unrestricted crystal experiment.

Fig 2 gives a dimensionless illustration with $t = T/T_{ref}$, S = 0.6, and a thermal coefficient of 0.4 at t = 1. The constructed amplitudes are 1.0 and 1.4 at t = 1 and t = 2. One measurement admits a line of amplitude pairs; the second intersects that line at a single pair. These numbers have no empirical connection to the Si or Ge measurements. Their purpose is to display the change in the observation geometry.

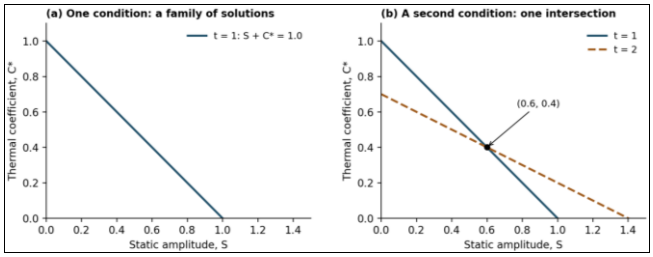


Fig 2: An independent contrast can remove an amplitude ambiguity

Note: Constructed example with $t = T/T_{ref}$ and $C^* = CT_{ref}$. The model is $Y = S + C^* t$. Panel (a) uses Y(1) = 1.0; panel (b) adds Y(2) = 1.4, selecting S = 0.6 and C* = 0.4. Axes show nonnegative amplitudes. Background, normalization, and the assumed temperature law are treated as known or controlled. No historical temperature measurements are represented.

An unknown temperature-independent background changes the conclusion. With Y(T) = S + B + CT, temperature measurements identify the intercept S + B and the slope C, but do not separate S from B. More temperatures improve estimation of the intercept without resolving its decomposition. Similarly, an unconstrained normalization factor for every temperature can absorb changes that would otherwise identify the thermal coefficient. The experimental contrast supplies useful information only when those additional degrees of freedom are constrained.

A related local nuisance example makes this explicit. If the recorded response is $y(q) = a_s f_s(q) + a_t f_t(q) + B$, its amplitude sensitivity columns are f_s and f_t, while the background sensitivity is the constant function 1. Even two distinct profiles may become poorly distinguishable after background is allowed to vary when much of their difference lies in a constant offset over the sampled angular window. Similarly, a free angular-zero shift contributes a local sensitivity proportional to the derivative of the predicted profile and can absorb a small feature displacement. A claimed improvement in separation should therefore be checked after nuisance projection, not solely from the rank of the two-profile matrix. This is an analytical implication, not a fitted sensitivity result for the 1986 apparatus.

The same reasoning organizes other proposed measurements. Energy analysis adds contrast through the different energy-transfer distributions of elastic and inelastic processes. Reflection and azimuth changes can exploit different directional responses. Surface interventions can compare sensitivity to preparation, but their interpretation requires a joint model for the effects they may change. Table 3 links these contrasts to the ambiguity each is intended to address. The analysis does not rank them numerically because neither complete competing forward models nor the required uncertainty budgets are available for the historical experiment.

The contrast-selection principle can be expressed operationally: First specify at least two plausible complete forward models; next propagate both through the same energy and angular acceptance; then identify where their predictions differ beyond the adjustments permitted to normalization, zero angle, background, and resolution; finally choose additional measurements that maximize that remaining difference within feasible uncertainty. Energy analysis is often conceptually direct for elastic versus inelastic scattering, but low-energy phonons and finite analyzer resolution may remain unresolved. Directional scans may distinguish predicted polarizations or surface-normal signatures, provided absolute or calibrated relative scale links are preserved between scans.

Table 3: Experimental contrasts and the ambiguities they can address

Added contrast	Potential distinguishing information	Necessary constraints
Temperature series	Different thermal and temperature-independent responses	Validate temperature law; register angle; monitor flux; constrain background
Energy-transfer analysis	Elastic versus resolved inelastic intensity	Calibrate energy response; account for unresolved low-energy scattering
Reflections or azimuths	Different polarization, strain, and surface-direction responses	Use shared physical parameters and calibrated relative intensities
Surface intervention	Sensitivity to modified near-surface structure	Measure alignment, strain, relief, and illuminated geometry as relevant
Instrument or reference scans	Features generated by the optical arrangement	Match angular and spectral acceptance; characterize response wings
Repeat scans and longer counting	Better precision and tests of drift or reproducibility	Do not expect repeats alone to remove exact component degeneracy

Note: Prospective methodological synthesis. No row is claimed to have been implemented as an additional experiment in the thesis, and no optimal ordering is established.

5. Discussion

The principal result is a clarification of the inferential meaning of the historical evidence. A measured feature can be repeatable, preparation-sensitive, and inconsistent with a simple benchmark while its microscopic composition remains non-unique. These statements are compatible. Repeatability concerns the stability of the observable, benchmark failure concerns a specified prediction, and mechanism identification concerns discrimination among admissible alternatives. Treating them as equivalent risks assigning more physical specificity to a diffraction curve than its observation scheme supports.

This clarification also changes how the original thermal comparison should be discussed. A q-dependent kinematical approximation and a dynamical thermal-scattering calculation are different forward models. Structured thermal responses calculated near a Bragg condition do not invalidate the thesis observations, but they enlarge the set of

physically plausible alternatives [5, 6]. A secondary synthesis should preserve the original comparison while stating the assumptions under which it was informative. Rejecting that comparison does not measure a zero phonon contribution.

Surface treatment supplies a useful intervention because it changes the specimen rather than merely repeating the scan. Nevertheless, its causal specificity is limited. Rubbing or polishing can affect defect distributions and surface relief, but also strain, illuminated geometry, and the coupling of radiation to the crystal. Modern surface-relief theory reinforces the need to account for geometry in the forward model [11]. The preparation contrast supports surface sensitivity most directly. A quantitative defect-density interpretation would require an independently justified relation between defect population and measured response.

The exact common-response example explains why increased counting precision cannot solve every attribution problem. When the forward map contains only an amplitude sum, a smaller error on that sum does not constrain its partition. The Gaussian example addresses a different situation: Small shape differences exist, but their information can be suppressed by broadening. There, improved resolution, a wider informative sampling range, or additional counts can improve estimation, provided the differences survive calibration uncertainty. The distinction prevents structural ambiguity from being mistaken for an ordinary shortage of photons.

Instrument characterization is therefore part of mechanism inference. A peak-like residual should be tested against plausible optical origins, especially in a multi-crystal arrangement where a secondary feature can be generated at a crystal other than the specimen [4]. Response measurements should cover the wings and relevant angular–spectral acceptance, not only quote a central width. Lucas *et al*. [14] provide an experimental precedent for examining this broader response. Uncertainty in an instrumental tail can be strongly correlated with the amplitude of a weak specimen component.

For a nonlinear joint analysis, the relevant question is whether target-parameter sensitivities remain independent after changes achievable by nuisance parameters have been allowed. A temperature-induced shift that resembles an alignment drift provides less discriminatory information when the zero angle is unconstrained. A treatment-dependent height change may be absorbed by an unknown illuminated area. An apparent improvement in fit obtained by adding a free amplitude to every scan does not necessarily improve the identification of a shared physical mechanism. Joint experiments need shared parameters justified by physics, together with explicit condition-specific nuisance terms.

For a joint data set with multiple reflections or temperatures, one should declare in advance which quantities are physically shared across conditions. For example, a common defect-related parameter may predict changes across several reflections, whereas detector normalization and angular-zero offsets may vary by acquisition. If every curve is assigned unconstrained component amplitudes and independent backgrounds, the additional data may increase flexibility rather than identify a mechanism. A useful reporting practice would include the singular values or profile-likelihood intervals for target parameters both before and after nuisance optimization, together with held-out-condition predictions where measurements permit.

Temperature dependence is attractive because it can generate a contrast different from angular position. However, the linear CT model applies only within an appropriate classical regime and after relevant corrections. Thermal expansion, Debye–Waller changes, occupation factors outside the classical limit, and possible changes in static disorder can alter the response. Measurements on heating and cooling, registered reference reflections, flux monitoring, and independent background observations help assess these effects. The temperature example demonstrates the logic of an additional independent equation; it does not prescribe a universal two-temperature separation method.

Energy discrimination offers a more direct way to address the elastic–inelastic distinction, but it too has finite resolving power. An energy-integrating counter cannot establish that a weak angular peak is elastic. Conversely, an elastic energy window of finite width can include unresolved quasielastic or low-energy contributions. Phonon-sensitive diffraction work illustrates the value of measurements designed around the relevant momentum and energy scales [18, 19]. The appropriate measurement depends on the predicted energy-transfer distribution and the calibrated energy response, not merely on the presence of an analyser crystal.

Reciprocal-space coverage is another useful discriminator because the same radial dependence can coexist with different directional patterns. Surface truncation, defect strain, and phonon polarization need not produce the same variation around a reciprocal-lattice point. Robinson [10] illustrates the importance of directional extension for surface-related scattering. Multiple reflections or azimuths can consequently add information that repeated sampling along one line lacks. Their value is reduced if independent scale factors and unconstrained component shapes are introduced for every new scan, eliminating the physical links that were meant to distinguish mechanisms.

Model adequacy must remain separate from identifiability throughout this process. A unique best fit within a narrow family can still be physically misleading if an important contribution is omitted. Conversely, a broad family of statistically acceptable fits may honestly represent the information in the data. Sensitivity analysis and profile likelihood can help locate ambiguous parameter directions, but they cannot certify that every relevant physical alternative has been included [15, 16]. Residual structure, prediction under held-out experimental conditions, and consistency with independent characterization provide complementary tests.

The synthesis has several limitations. The archival examples concern particular specimens, reflections, and historical optics, so their qualitative interpretation should not be generalized into universal amplitude laws. The analytical illustrations use simplified linear models and ideal inner products; actual Poisson counting, finite sampling, parameter bounds, and correlated errors would require a likelihood appropriate to the measurements. No resolution kernel, phonon spectrum, or defect distribution has been inferred anew. The proposed contrasts are therefore a framework for planning a discriminating experiment, rather than evidence that the original mechanism question has now been resolved.

An additional limitation concerns physical realism. The Gaussian shapes and the S + C T example were chosen to isolate mathematical aspects of inverse inference. They should not be read as approximations validated for the

specific Si 220 or Ge 111 optical geometries. The anisotropic $|q|^{-2}$ expressions discussed in the theoretical section likewise illustrate possible directional non-equivalence rather than a new fit or a material-specific scattering calculation. A full diffraction simulation would need elastic constants, crystal thickness, boundary conditions, specimen disorder, instrumental transmission, and appropriate coherent or incoherent coupling. These inputs are not presently recoverable from the summarized archive, so no apparent new empirical precision is claimed.

The methodological contribution is to connect every proposed measurement to an explicit ambiguity. If two models predict the same measured angular function, repeating that observable is insufficient for unique separation. If they differ mainly in energy transfer, energy analysis is relevant. If they differ in direction, reciprocal-space coverage is relevant. If their thermal response differs, temperature contrast is relevant only with the accompanying nuisance controls. This connection makes experimental planning more precise: The next measurement should change the relative predictions in a way that cannot be reproduced by admissible changes in alignment, scale, background, or instrument response.

This framework also specifies what would count as a stronger future test. A convincing mechanism attribution should compare at least two physically admissible models against jointly calibrated counts, report the effect of uncertain instrumental response on the inferred component proportions, and seek independent validation through energy, directional, or intervention contrasts selected on the basis of model predictions. A sharply defined model may fit exceptionally well yet fail under another reflection or energy window; conversely, several mechanisms may remain observationally equivalent despite excellent repeatability. Explicitly reporting that equivalence is a substantive scientific result, not a failure to interpret the experiment.

6. Conclusion

The archival near-Bragg observations provide evidence of preparation-sensitive diffraction features and challenge the particular angular thermal-scattering benchmark tested historically. They do not by themselves identify a unique defect mechanism or determine elastic and inelastic intensity fractions. The strength of the present reassessment is therefore methodological: It specifies the inferential boundary between an observed mismatch, parameter estimability within a model, and discrimination among competing physical explanations after instrumental transformation.

The constructed analyses show that identical recorded component responses determine only their amplitude sum and that nearly coincident profiles create unstable decompositions under the specified ideal metric. Temperature contrast can separate two amplitudes only when the temperature law, normalization, and background are constrained. Extending the analysis to nuisance sensitivities makes clear why a formally full-rank two-component model need not remain informative when background, angular zero, or resolution can change concurrently.

Future near-Bragg experiments should therefore select calibrated contrasts according to the particular degeneracy they can break: Energy-transfer measurements for elastic–inelastic differences, multiple directions or reflections for anisotropic responses, reference scans for instrumental structure, and controlled temperature or surface interventions for conditional mechanism tests. Where feasible, joint physical forward modeling and nuisance-aware sensitivity analysis should precede mechanistic claims. Historical data remain valuable in motivating and delimiting these questions, but the constructed examples presented here are not substitutes for material-specific simulations or new measurements.

7. Author's Note

Following my retirement after more than four decades of academic service, I have returned to the experimental research conducted during my doctoral studies in the 1980s. The primary historical sources for this article are my 1986 doctoral dissertation at the University of Ioannina and the associated scientific publications produced during that period. These materials provide the original experimental observations, diffraction geometries, and interpretations upon which the present reassessment is based.

The historical findings are reconsidered in the light of subsequent developments in dynamical X-ray diffraction, diffuse scattering, instrumental characterization, and mathematical identifiability. The analytical models and illustrative calculations introduced in this article were developed for the present study and must not be interpreted as newly recovered measurements or quantitative reconstructions of the original experiments.

This retrospective investigation seeks to preserve the scientific value of the historical observations while critically examining their interpretative limitations and identifying questions that remain unresolved. By explicitly distinguishing original experimental evidence, previously published interpretations, subsequent scientific developments, and new theoretical analyses, the article aims to ensure transparency regarding the provenance and scientific status of its findings.

8. References

1. Kotsis KT. Dynamiki kai kinimatiki skedasi ton aktinon-X konta se simeio tou antistrofou plegmatos [Dynamical and kinematical X-ray scattering near a reciprocal-lattice point] [doctoral dissertation, University of Ioannina]. National Archive of PhD Theses, 1986. Doi: 10.12681/eadd/0880
2. Alexandropoulos NG, Kotsis KT. Use of kinematical diffraction in X-ray topography. Journal of Applied Crystallography. 1985; 18(6):509-512. Doi: 10.1107/S0021889885010792
3. Kotsis KT, Alexandropoulos NG. Diffraction pattern near the Bragg angle for an asymmetrically cut crystal. Journal of Applied Crystallography. 1986; 19(6):473-476. Doi: 10.1107/S0021889886088921
4. Kotsis KT, Alexandropoulos NG. A source of spurious peaks in a multi-crystal X-ray spectrometer. Journal of Physics E: Scientific Instruments. 1987; 20(1):74-76. Doi: 10.1088/0022-3735/20/1/013
5. Juretschke HJ. Thermal diffuse scattering within a Bragg peak. Acta Crystallographica Section A: Foundations of Crystallography. 1985; 41(6):598-603. Doi: 10.1107/S0108767385001301
6. Mitsui T, Fujiwara K, Imai Y, Yoda Y. Dynamical effects on thermal diffuse scattering in Si 111 Bragg reflection. Journal of the Physical Society of Japan.

2022; 91(3):035002. Doi: 10.7566/JPSJ.91.035002
7. Batterman BW, Cole H. Dynamical diffraction of X rays by perfect crystals. Reviews of Modern Physics. 1964; 36(3):681-717. Doi: 10.1103/RevModPhys.36.681
8. Guigay JP, Sanchez del Rio M. Formulation of perfect-crystal diffraction from Takagi–Taupin equations: Numerical implementation in the crystalpy library. Journal of Synchrotron Radiation. 2024; 31(6):1469-1480. Doi: 10.1107/S160057752400924X
9. Dederichs PH. The theory of diffuse X-ray scattering and its application to the study of point defects and their clusters. Journal of Physics F: Metal Physics. 1973; 3(2):471-496. Doi: 10.1088/0305-4608/3/2/010
10. Robinson IK. Crystal truncation rods and surface roughness. Physical Review B. 1986; 33(6):3830-3836. Doi: 10.1103/PhysRevB.33.3830
11. Karpov AV, Kazakov DV, Punegov VI. Dynamical theory of X-ray diffraction by crystals with different surface relief profiles. Acta Crystallographica Section A: Foundations and Advances. 2023; 79(2):171-179. Doi: 10.1107/S2053273322012062
12. Wasserstein-Robbins F, Juretschke HJ. Dynamical effects in X-ray–thermal phonon interactions in symmetric Bragg reflections. Acta Crystallographica Section A: Foundations of Crystallography. 1985; 41(6):591-597. Doi: 10.1107/S0108767385001295
13. Schmidt EM, Thomas S, Bulled JM, Minelli A, Goodwin AL. Interplay of thermal diffuse scattering and correlated compositional disorder in $KCl_{1-x}Br_x$. Acta Crystallographica Section B: Structural Science, Crystal Engineering and Materials. 2022; 78(3):385-391. Doi: 10.1107/S2052520622003560
14. Lucas CA, Gartstein E, Cowley RA. The resolution function of an X-ray triple-crystal diffractometer: Comparison of experiment and theory. Acta Crystallographica Section A: Foundations of Crystallography. 1989; 45(6):416-422. Doi: 10.1107/S010876738900108X
15. Raue A, Kreutz C, Maiwald T, Bachmann J, Schilling M, Klingmüller U, *et al*. Structural and practical identifiability analysis of partially observed dynamical models by exploiting the profile likelihood. Bioinformatics. 2009; 25(15):1923-1929. Doi: 10.1093/bioinformatics/btp358
16. Wieland FG, Hauber AL, Rosenblatt M, Tönsing C, Timmer J. On structural and practical identifiability. Current Opinion in Systems Biology. 2021; 25:60-69. Doi: 10.1016/j.coisb.2021.03.005
17. Rothenberg TJ. Identification in parametric models. Econometrica. 1971; 39(3):577-591. Doi: 10.2307/1913267
18. Bosak A, Chernyshov D. On model-free reconstruction of lattice dynamics from thermal diffuse scattering. Acta Crystallographica Section A: Foundations of Crystallography. 2008; 64(5):598-600. Doi: 10.1107/S0108767308020060
19. Gopalakrishnan G, Holt MV, McElhinny KM, Spalenka JW, Czaplewski DA, Schülli TU, *et al*. Thermal diffuse scattering as a probe of large-wave-vector phonons in silicon nanostructures. Physical Review Letters. 2013; 110(20):205503. Doi: 10.1103/PhysRevLett.110.205503